A simple model for the cloud adjacency effect and the apparent bluing of aerosols near clouds

Popular Summary

In determining aerosol-cloud interactions, the properties of aerosols must be characterized in the vicinity of clouds. Numerous studies based on satellite observations have reported that aerosol optical depths increase with increasing cloud cover. Part of the increase comes from the humidification and consequent growth of aerosol particles in the moist cloud environment, but part comes from 3D cloud-radiative transfer effects on the retrieved aerosol properties. Often, discerning whether the observed increases in aerosol optical depths are artifacts or real proves difficult. The paper provides a simple model that quantifies the enhanced illumination of cloud-free columns in the vicinity of clouds that are used in the aerosol retrievals. This model is based on the assumption that the enhancement in the cloud-free column radiance comes from enhanced Rayleigh scattering that results from the presence of the nearby clouds. The enhancement in Rayleigh scattering is estimated using a stochastic cloud model to obtain the radiative flux reflected by broken clouds and comparing this flux with that obtained with the molecules in the atmosphere causing extinction, but no scattering.

A simple model for the cloud adjacency effect and the apparent bluing of aerosols near clouds

Alexander Marshak[1], Guoyong Wen[2], James A. Coakley, Jr.[3], Lorraine A. Remer[1], Norman G. Loeb[4], and Robert F. Cahalan[1]

[1] NASA – Goddard Space Flight Center, Climate and Radiation Branch, MD
[2] University of Maryland Baltimore County, MD
[3] Oregon State University, OR
[4] NASA Langley Research Center, Climate Science Branch, Hampton, VA

Correspondence
Alexander Marshak
tel. 301-614-6122
email: Alexander.Marshak@nasa.gov

Prepared for publication in JGR
"Yoram J. Kaufman symposium on aerosols, clouds and climate" issue

A simple model for the cloud adjacency effect and the apparent bluing of aerosols near clouds

Abstract

In determining aerosol-cloud interactions, the properties of aerosols must be characterized in the vicinity of clouds. Numerous studies based on satellite observations have reported that aerosol optical depths increase with increasing cloud cover. Part of the increase comes from the humidification and consequent growth of aerosol particles in the moist cloud environment, but part comes from 3D cloud-radiative transfer effects on the retrieved aerosol properties. Often, discerning whether the observed increases in aerosol optical depths are artifacts or real proves difficult. The paper provides a simple model that quantifies the enhanced illumination of cloud-free columns in the vicinity of clouds that are used in the aerosol retrievals. This model is based on the assumption that the enhancement in the cloud-free column radiance comes from enhanced Rayleigh scattering that results from the presence of the nearby clouds. The enhancement in Rayleigh scattering is estimated using a stochastic cloud model to obtain the radiative flux reflected by broken clouds and comparing this flux with that obtained with the molecules in the atmosphere causing extinction, but no scattering.

1. Introduction

Numerous studies based on satellite observations have reported a positive correlation between cloud amount and aerosol optical thickness (AOT) (e.g., Sekiguchi et al., 2003; Loeb and Manalo-Smith, 2005; Zhang et al., 2005, Kaufman et al., 2005a, Matheson et al., 2005). Recently, Koren et al. (2007), using MODIS data, showed that the average reflectance for cloud-free ocean scenes far away from clouds were up to 30% lower than those near cloud edges. The higher reflectances lead to higher AOTs retrieved in the vicinity of clouds. This positive correlation can be explained as a result of physical phenomena such as the humidification of aerosols in the relatively moist cloud environment or a transition between aerosol and clouds where the cloud signature is weak (evaporation and/or activation of cloud drops) and the distinction between cloudy and cloud-free air becomes problematic. The term "twilight zone" was coined by Koren et al. (2007) to describe the regions around clouds which are neither precisely cloud-free nor precisely cloudy. On the other hand, part of the correlation can result from remote sensing artifacts such as cloud contamination of the cloud-free fields of view used in the aerosol retrievals. Kaufman and Koren (2006) noted that any "satellite analysis may be affected by potential cloud artifacts."

There are two ways that clouds affect the retrievals of aerosols: (*i*) the existence of small amounts of sub-pixel sized clouds in pixels identified as being cloud-free and (*ii*) an enhancement in the illumination of the cloud-free column through the reflection of sunlight by nearby clouds. When the pixels are relatively large (e.g., TOMS ~ 40 km, OMI ~ 15 km), only the first type (unresolved variability), cloud contamination is considered (e.g., Torres et al., 2002; Sinyuk et al., 2003). The second type (resolved variability), also called the 'cloud adjacency effect,' is more pronounced when satellite pixels are relatively small (e.g., MODIS and MISR ~ 0.5 km). Kobayashi et al. (2000), Cahalan et al. (2001), Podgorny (2003), Wen et al., (2001, 2006, 2007), Nikolaeva et al. (2005) studied the cloud adjacency effect when cloud-free pixels are brightened (or shadowed) by reflected light from surrounding clouds using 3D radiative transfer calculations applied to LANDSAT, MODIS, and ASTER data as well as to numerically generated cloud fields including an isolated cubical cloud. Both cloud contamination and the cloud adjacency effect may substantially increase reflected radiation and thus lead to significant overestimates of the AOT. These two types of cloud effects, however, have different impacts on the retrieved AOT: sub-pixel clouds increase AOT by increasing the apparent contribution due to large particles (aerosol "coarse" mode), cloud adjacency mostly increases the apparent contribution due to small particles (aerosol "fine" mode). This short paper quantifies the second factor by using a simple stochastic cloud model to obtain the radiative flux reflected by broken clouds and comparing this flux with that obtained with the molecules in the atmosphere causing extinction, but no scattering.

The next section discusses the factors that contribute to the enhancement of a cloud-free column through the cloud adjacency effect. Section 3 introduces a simple two-layer model of the cloud enhancement with broken clouds as the lower layer and molecular scattering as the upper layer. A Poisson stochastic cloud model used to obtain the upward flux reflected by broken clouds is briefly described in Section 4. Section 5 compares the results of this simple model with those obtained from Monte Carlo calculations for broken cumulus clouds over Brazil observed by MODIS. Finally, Section 6 summarizes the results and discusses their implications.

2. Cloud enhancement and its contributors

Current methods used to retrieve AOT in cloud-free pixels account for sunlight reflected by the underlying surface and by the Rayleigh scattering due to molecules in the atmosphere but not the sunlight reflected by surrounding clouds. Sunlight reflected by the surrounding clouds, however, is an additional source of radiation that reaches the sensor as a result of (*i*) reflection by the underlying surface, (*ii*) scattering by the aerosol, and (*iii*) scattering by molecules. The relative roles of these three contributions varies from scene to scene and depends on many factors, including wavelength, surface reflectance, nearest cloud distance, cloud optical depth, the vertical and horizontal distributions of clouds, AOT, the vertical distribution of aerosols (relative to clouds), the solar and satellite viewing angles.

Wen et al. (2006, 2007) gained insight into the cloud adjacency effect by performing synthesized aerosol retrievals in realistic broken cumulus fields over a biomass burning region in Brazil as observed by MODIS. They assumed that all aerosols were below the cloud tops and used 3D and 1D radiative transfer calculations to determine the average difference between the 3D and 1D reflectances for all cloud-free pixels as given by

$$\Delta\rho = \overline{r_{3D}(x,y) - r_{1D}}\,. \tag{1}$$

The calculations were performed for a variety of surface albedos and 3 different AOTs, 0.1, 0.5 and 1.0 at different wavelengths. They referred to $\Delta\rho$ as the 'cloud-induced enhancement' or just 'cloud enhancement.' Figure 1 illustrates the results calculated for the 0.47 μm wavelength. For dark surfaces the enhancement is not sensitive to AOT. For bright surfaces, the enhancement decreases with AOT because the aerosol layer prevents photons reflected by the surface from reaching the satellite. The intercept with the vertical axis gives the enhancement for zero surface albedo and thus provides estimates for the contribution from Rayleigh scattering. The contribution from molecular scattering dominates over aerosol scattering which, as is evident from the figure, is nearly an order of magnitude smaller even for an AOT of 1. The relative roles of molecular and aerosol scattering arise because the scattering angles encountered in the retrievals of aerosol properties are typically between 100° and 150°. For this the range of angles the normalized phase functions for aerosols are much smaller than the Rayleigh phase function (e.g., Liou, 2002, p. 98).

In summary, for dark surfaces and low-level clouds with aerosols below the cloud layer, sunlight reflected by the clouds and then scattered by molecules in the cloud-free columns is the key process for the enhancement of retrieved AOT, at least for the shorter wavelengths at which Rayleigh scattering is strong. Since the enhancement is due primarily to Rayleigh scattering and not very sensitive to AOT, the enhancement can be assessed knowing only the cloud properties and the (average) distance from a cloud-free pixel to a cloudy pixel.

3. A simple model for the cloud-induced enhancement of reflectances for nearby cloud-free columns

Assume that the enhancement of the reflectance in the cloud-free column is due *entirely* to Rayleigh scattering. Consider a simple, two-layer model with broken clouds in the lower layer and a layer of molecules for the upper layer (Fig. 2). Take the cloud enhancement to be the difference between the following two radiances: (a) one is reflected from a broken cloud field with a scattering Rayleigh layer above it and (b) one is reflected from the same broken cloud field but with the molecules in the upper layer causing extinction, but no scattering. In other words,

$$\Delta\rho = r_1 - r_2 \tag{2}$$

where

$$r_1(\theta_0,\theta) = R_m(\theta_0,\theta) + \frac{\alpha_c(\tau,\theta_0)T_m(\theta_0)t_m(dif,\theta)}{1-\alpha_c(\tau,\theta_0)R_m(dif)} \tag{3}$$

and

$$r_2(\theta_0,\theta) = R_m(\theta_0,\theta) + \alpha_c(\tau,\theta_0)T_m(\theta_0)t_m(dif,\theta). \tag{4}$$

Here sub-index 'm' stands for 'molecule' while 'c' stands for 'cloud.' $R_m(\theta_0,\theta)$ is the reflectance for a molecular layer with no clouds below (this term is irrelevant here since it is canceled in calculating $\Delta\rho$). Cloud reflectance, α_c, is the critical parameter in this simple model because, in addition to cloud optical depth, τ, and SZA, θ_0, it is also a function of the cloud brokenness as will be discussed below. T_m is the transmittance through the molecular layer with direct sunlight incident from above while t_m is the transmission through the molecular layer for diffuse illumination from below. Finally, $R_m(dif)$ is the reflectance of the molecular layer illuminated by diffuse radiation from below. Note that with the exception of α_c, all the quantities in (2)-(4) are 1D and are calculated using a standard plane-parallel radiative transfer code. For simplicity, the surface is assumed to be black. Contributions from non-zero surface reflectances can be readily included in α_c.

In summary, a simple two-layer model with a broken cloud field below and Rayleigh scattering molecular layer above is used to quantify the cloud-induced enhancement of Rayleigh scattering. The enhancement comes from the enhanced illumination of the molecular layer through the reflection of sunlight by the surrounding clouds. The main unknown is the reflectance for a broken cloud field. If we assume that the clouds are plane-parallel rather than broken then α_c will be overestimated. Since $\Delta\rho$ in (2)-(4) is an increasing function with respect to α_c (Fig. 3), the plane-parallel approximation will also overestimate the effect of clouds on cloud-free pixels.

The next section will describe the calculation of α_c for a broken cloud field using a stochastic model. The advantage of using a stochastic model is that the output is 'generic.' It is averaged over many realizations of a cloud field with given statistical properties.

4. The Poisson stochastic model for broken clouds

The one-layer Poisson model for broken clouds originally proposed by Titov (1991) is used to calculate the cloud reflectance for broken cloudy regions. Kassianov (2003) generalized this one-layer model to multilayer broken cloud fields while Zhuravleva and Marshak (2005) validated the one-layer model by comparing results with those generated using fractal cloud fields. The main parameters in the model are as follows: (*i*) cloud fraction, A_c, (*ii*) averaged cloud optical depth τ, and (*iii*) cloud aspect ratio, γ, which is defined as the ratio of cloud vertical to horizontal dimensions. In addition, the single scattering albedo and the cloud droplet scattering phase function along with the surface albedo are specified. For the shortwave calculations performed here, the droplet single-scattering albedo is set to unity and the C1 phase function (Deirmendjian, 1969) was used. Figure 4 shows an example of two broken cloud fields with $A_c = 0.3$ and $\gamma = 0.5$ and 1.

The output of the stochastic model is the domain (and ensemble) averaged upward and downward fluxes with downward fluxes subdivided into diffuse and direct components. Zhuravleva and Marshak (2005) used these subdivided fluxes to determine cloud aspect ratios from ground-based measurements.

Note that two (averaged cloud optical depth, τ, and cloud fraction, A_c) out of the three principal input parameters can be determined from the MODIS Cloud Product (MOD06). The third parameter (cloud aspect ratio γ) is not readily available. Fortunately, as is shown in the next section, the cloud enhancement is not very sensitive to the aspect ratio, at least for small solar zenith angles.

A simple one-layer stochastic model is used to derive cloud reflectances as a function of the average cloud optical depth, cloud fraction, and cloud aspect ratio for broken cloud regions. The clouds are distributed in space according to a Poisson distribution so that the average distance from a cloud-free pixel to a cloud edge is uniquely determined by cloud fraction and cloud aspect ratio.

5. Results

Figure 5 shows the cloud-induced enhancement Δρ as a function of cloud optical depth for 0.47 μm and four cloud fractions: $A_c = 1.0$, 0.7, 0.5, and 0.3. The aspect ratio $\gamma = 1$, the solar zenith angle $\theta_0 = 60°$, the view zenith angle $\theta = 0°$, and the surface albedo, $\alpha_s = 0.0$. Note that the case of $A_c = 1.0$ represents unbroken clouds and corresponds to the plane-parallel approximation. The figure depicts an example of a look-up-table (LUT) that can be used to estimate the expected enhancement of cloud-free radiances in the vicinity of clouds. Consider a broken cloud scene with 70% cloud cover and an average cloud optical depth of 22 illuminated by the sun with a zenith angle of 60°. The enhancement in Rayleigh scattering at 0.47 μm in the nadir direction will likely be 0.04 larger than its 1D counterpart.

To assess the merits of the above approach, estimates of the cloud enhancement were made for the two 68 by 80 km broken cloud scenes in biomass-burning regions of Brazil studied by Wen et al. (2007). Both scenes were simultaneously observed by MODIS and ASTER. The first cloud scene (centered at 0.0N, 53.78W and acquired on Jan. 25, 2003) was described by Wen et al. (2006) while the retrieved cloud parameters for the second scene (centered at 17.1S, 42.16W and acquired on Aug. 9, 2001) were described and analyzed by Marshak et al. (2006).

The first scene had cloud fraction $A_c = 0.53$ and cloud optical depth $\tau = 12$ (std = 10), and the solar zenith angle was $\theta_0 = 32°$. The surface was covered by vegetation with a low albedo of 0.011 at 0.47 μm and 0.025 at 0.65 μm. For this scene, Wen et al. (2007) found an average cloud enhancement of 0.015 (std = 0.005) at 0.47 μm and 0.004 (std = 0.008) at 0.65 μm (marked as 'squares' in the left panel of Fig. 6). Two 15 by 15 km subsets of this scene with thick ($\tau = 14$, std = 8, and $A_c = 0.59$) and thin ($\tau = 7$, std = 6, and $A_c = 0.51$) broken clouds were also examined using high-resolution cloud fields retrieved from ASTER data in 3D Monte Carlo simulations of the radiance fields. The cloud-induced enhancement was found to be 0.019 and 0.012 at 0.47 μm for thick and thin clouds and 0.01 and 0.0018 at 0.65 μm (marked as 'circles' in the left panel of Fig. 6). In addition, Fig. 6 shows asymptotic values (marked as 'ovals' in the left panel of Fig. 6) corresponding to the enhancements at the largest distances from cloud edges. At the greatest distances from the clouds, cloud shadows are generally avoided thereby giving a more representative estimate of the 3D effects than that obtained by averaging over all of the cloud-free pixels, some being darkened by shadows.

The second scene had cloud fraction, $A_c = 0.4$ and cloud optical depth, $\tau = 8$ (std = 8) and solar zenith angle, $\theta_0 = 41^\circ$ (right panel of Fig. 6). The surface was much more heterogeneous than the surface for the first scene. It was also much brighter at shorter wavelengths with an average albedo of 0.04 at 0.47 μm, 0.07 at 0.65 μm (and 0.2 at 0.84 μm.) For this scene, Wen et al. (2007) found an asymptotic cloud enhancement of 0.006 at 0.47 μm and 0.003 at 0.66 μm ('ovals') at a distance of about 3 km from the cloud edges. The average values ('squares') for the cloud-free pixels selected by the MODIS AOT retrieval algorithm (Remer et al., 2005) have been included.

As the results in Fig. 6 indicate, the estimates based on the stochastic model can serve as a good first-order approximation to the cloud-induced enhancement calculated with a Monte Carlo code. The stochastic model underestimates somewhat the enhancement, at least for the particular scenes studied. Clearly, the enhancement is much smaller than would be obtained with a plane-parallel approximation ($A_c = 1$).

The left panel of Fig. 6 also illustrates the sensitivity of the modeled cloud enhancement, $\Delta\rho$, to cloud aspect ratio. For three wavelengths (0.47, 0.65, and 0.84 μm) and cloud fraction $A_c = 0.6$ the cloud enhancement as a function of optical depth τ is given for three cloud aspect ratios: $\gamma = 0.5, 1, 2$. For a fixed cloud geometrical thickness of 1 km, this means that the average cloud horizontal dimension varies from 500 m to 2 km. The uncertainties caused by an unknown (but reasonable) aspect ratio are of the order of 5-10%. For small cloud fractions and large solar zenith angles the modeled enhancements become more sensitive to cloud aspect ratio.

The right panel of Fig. 6 also shows the effect of surface albedo. For small cloud fraction the contribution of a bright surface to the total cloud-induced enhancement can be significant. It is interesting to note that, in contrast to plane-parallel clouds, the surface contribution to the total enhancement does not decrease with cloud optical depth. It is almost constant. This is a special feature of broken cloud fields where the radiation reflected by the surface in cloud-free regions goes directly to a satellite detector rather than being attenuated by the clouds.

Finally, the effect of the enhancement on the Angström exponent in the vicinity of clouds is studied. The Angström exponent characterizes the dependency of aerosol optical thickness on wavelength and is related to the average size of the particles in the aerosol: the smaller the particles, the larger the exponent.

Consider three cases with the "true" Angström exponents equal to 0 for a "clean" environment, 1.04 for a "polluted" environment, and 2.14 for a "very polluted" environment for 0.47 and 0.65 μm, and 0, 1.31, and 2.7 for 0.65 and 0.84 μm. The clean case with zero Angström exponent indicates that the extinction is independent of wavelength, as it is for clouds and for large nonabsorbing aerosols, like sea salt. The AOT is taken to be 0.1 at 0.65 μm. Taking into account the cloud-induced enhancement, the "apparent" Angström exponent will be greater than zero. Figure 7 illustrates the increase in Angström exponents for both spectral intervals. Obviously, for highly polluted environments, the cloud adjacency effect is much smaller than for clean environments. Nonetheless, owing to the effects of clouds, the retrieved Angström exponent can be substantially larger than its true value. The cloud adjacency effect is opposite that for cloud contamination where subpixel scale clouds increase the "coarse" mode fraction thereby decreasing the Angström exponent.

6. Summary and discussion

A simple model was described for estimating the cloud-induced enhanced reflectances of cloud-free columns in the vicinity of clouds. The enhancement was assumed to be due entirely to Rayleigh scattering. For the shorter wavelengths where molecular scattering is relatively large, attributing the enhancement to the illumination of the Rayleigh scattering atmosphere by sunlight reflected from nearby clouds proved reasonable (Fig. 1) for scenes with dark surfaces, broken, low-level cumulus clouds, and an aerosol layer below the cloud tops. The enhancement in Rayleigh scattering was estimated using a stochastic cloud model (Fig. 4) to obtain the radiative flux reflected by broken clouds and comparing this flux with that obtained with the molecules in the atmosphere causing extinction, but no scattering as given by (2)-(4).

The results of numerical simulations of the enhancement (Wen et al. 2007) were shown to be in good agreement (Fig. 6) with the simple model, although the model underestimates somewhat the enhancement for the particular scenes studied, cumulus cloud fields retrieved from collocated MODIS and ASTER images over a biomass burning region in Brazil.

The one-layer Poisson stochastic cloud model (Titov, 1990) uses cloud optical depth, τ, droplet single scattering albedo and scattering phase function, cloud fraction, A_c, cloud aspect ratio, γ, and surface albedo to estimate reflectances for broken cloud fields. The optical depth and cloud fraction are given in the MODIS Cloud Product (MOD06). They can be used as a first approximation to quantify the cloud-induced enhancement from precalculated look-up-tables (see Fig. 5, for an example). The cloud aspect ratio is not readily available but the error due to an incorrect cloud aspect ratio is 5-20%. For clouds distributed in space according to a Poisson distribution, the average distance from a cloud-free pixel to the nearest cloud is uniquely determined by cloud fraction and cloud aspect ratio.

The assumption that the enhancement of the cloud-free column is due to molecular scattering leads naturally to a larger increase of AOT for shorter wavelengths, or to a "bluing" of aerosols near clouds (Fig. 7). As a result, in contrast to cloud contamination by sub-pixel clouds, the cloud adjacency effect will increase the apparent aerosol "fine" mode fraction rather than the "coarse" mode fraction. Recent findings in the MODIS cloud and aerosol products indicate that the AOT and its fine mode fraction increase in the vicinity of clouds (Kaufman et al., 2005b).

Since MODIS and CERES are on the same spacecraft, another approach to estimating spectral upward fluxes for broken cloud fields is to use the CERES data. Using CERES fluxes rather than a stochastic cloud model requires the use of a theoretical radiative transfer model to convert broadband fluxes to spectral fluxes. A simpler approach would be to ignore the wavelength dependence in the anisotropy as given by the CERES Angular Distribution Models (ADMs) (Loeb et al. 2005) and use the ADMs to determine spectral fluxes from the MODIS radiances. This approach, however, can lead to the large errors at the 10 by10 km scale of the MODIS Aerosol Product and needs further study.

The enhanced illumination of cloud-free columns is a key part of characterizing aerosol properties in the vicinity of clouds. In satellite based studies of cloud-aerosol interactions, changes in the properties of the aerosol due to the cloud environment must be separated from the apparent changes that come from 3D cloud-radiative transfer effects on the retrieved aerosol properties.

The simple model presented here should be taken as limited to the case of low-level clouds over dark surfaces with the aerosol below the cloud tops. The model may well prove inappropriate for scenes with highly reflecting surfaces, with upper-level clouds, or in which a substantial fraction of the aerosol lies above the low-level clouds. In such cases molecular scattering will not necessarily have the dominant role that it has for the low-level cloud and aerosol systems studied here.

Acknowledgments. This work was supported by the Department of Energy (under grant DE-AI02-95ER61961 to NASA's GSFC) as part of the Atmospheric Radiation Measurement (ARM) program, and by NASA's Radiation Program Office (under grants 621-30-86 and 622-42-57). We thank C. Chiu, A. Davis, I. Koren, T. Varnai, and W. Wiscombe for stimulating discussions.

References

Cahalan, R. F., L. Oreopoulos, G. Wen, A. Marshak, S.-C. Tsay, and T. DeFelice, 2001: Cloud Characterization and Clear Sky Correction from Landsat 7. *Remote Sens. Environ.*, **78**, 83-98.

Deirmendjian, D., 1969: *Electromagnetic Scattering on Spherical Polydispersions*. Elsevier, New York (NY), 292 pp.

Kassianov E., 2003: Stochastic radiative transfer in multilayer broken clouds. Part I: markovian approach. *J. Quant. Spectrosc. Radiat. Transfer*, **77**, 373-394.

Kaufman, Y.J., L.A. Remer, D. Tanre, R.R. Li, R. Kleidman, S. Mattoo, R. Levy, T. Eck, B.N. Holben, C. Ichoku, J. Martins, and I. Koren, 2005a: A critical examination of the residual cloud contamination and diurnal sampling effects on MODIS estimates of aerosol over ocean. *IEEE Trans. Geosci. Remote Sens.*, **43**, 2886-2897.

Kaufman, Y. J., I. Koren, L. A. Remer, D. Rosenfeld, and Y. Rudich, 2005b: The effect of smoke, dust and pollution aerosol on shallow cloud development over the Atlantic ocean. *Proceedings of the National Academy of Sciences*, 10.1073/pnas.0505191102.

Kaufman, Y.J., and I. Koren, 2006: Smoke and pollution aerosol effect on cloud cover, *Science*, **313**, 655-658.

Kobayashi T., K. Masuda, M. Sasaki, J. Mueller, 2000: Monte Carlo simulations of enhanced visible radiance in clear-air satellite fields of view near clouds. *J. Geophys. Res.*, **105**, 26569-26576.

Koren, I., L. A. Remer, Y. J. Kaufman, Y. Rudich, and J. V. Martins, 2007: On the twilight zone between clouds and aerosols. *Geophys. Res. Lett.*, **34**, L08805, doi:10.1029/2007GL029253.

Liou, K. N., 2002: An introduction to atmospheric radiation. Academic Press, New York, 583 pp.

Loeb, N. G., and N. Manalo-Smith, 2005: Top-of-atmosphere direct radiative effect of aerosols over global oceans from merged CERES and MODIS observations. *J. Climate*, **18**, 3506-3526.

Loeb, N. G., S. Kato, K. Loukachine, and N. M. Smith, 2005: Angular distribution models for top-of-atmosphere radiative flux estimation from the Clouds and the Earth's Radiant Energy System instrument on the *Terra* satellite. Part I: Methodology. *J. Atmos. Oceanic Technol.*, **22**, 338–351.

Matheson, M.A., J.A. Coakley, Jr., and W.R. Tahnk, 2005: Aerosol and cloud property relationships for summertime stratiform clouds in the northeastern Atlantic from AVHRR observations. *J. Geophys. Res.*, **110**, D24204, doi:10.1029/2005JD006165.

Marshak, A., S. Platnick, T. Varnai, G. Wen, and R. F. Cahalan, 2006: Impact of 3D radiative effects on satellite retrievals of cloud droplet sizes, *J. Geophys. Res.*, **111**, DO9207, doi:10.1029/2005JD006686.

Nikolaeva, O.V., L. P. Bass, T. A. Germogenova, A. A. Kokhanovisky, V. S. Kuznetsov, and B. Mayer, 2005: The influence of neighboring clouds on the clear sky reflectance with the 3-D transport code RADUGA, *J. Quant. Spectrosc. Radiat. Transf.*, **94**, 405–424.

Podgorny, I.A., 2003: Three-dimensional radiative interactions in a polluted broken cloud system. *Geophys. Res. Lett.*, **30**, 1771, doi:10.1029/2003GL017287.

Remer, L. A., and 12 other coauthors, 2005: The MODIS aerosol algorithm, products, and validation, *J. Atmos. Sci.*, **62**, 947-973.

Sekiguchi, M., T. Nakajima, K. Suzuki, K. Kawamoto, A. Higurashi, D. Rosenfeld, I. Sano, S. Mukai, 2003: A study of the direct and indirect effects of aerosols using global satellite data sets of aerosol and cloud parameters. *J. Geophys. Res.*, **108**(D22), 4699, doi:10.1029/2002JD003359.

Sinyuk A., O. Torres, and O. Dubovik, Imaginary refractive index of desert dust using satellite and surface observations, 2003: *Geophys. Res. Letters,* **30** (2), 1081, doi: 10.1029/2002GL016189.

Titov, G. A., 1990: Statistical description of radiation transfer in clouds. *J. Atmos. Sci.*, **47**, 24–38.

Torres, O., P.K. Bhartia, J.R. Herman, A. Syniuk, P. Ginoux, and B. Holben, 2002: A long term record of aerosol optical depth from TOMS observations and comparison to AERONET measurements, *J. Atm. Sci.,* **59**, 398-413.

Wen, G., R. F. Cahalan, T.-S. Tsay, and L. Oreopoulos, 2001: Impact of cumulus cloud spacing on Landsat atmospheric correction and aerosol retrieval. *J. Geophys. Res.*, **106**, 12129-12138.

Wen, G., A. Marshak, and R. F. Cahalan, 2006: Impact of 3D clouds on clear sky reflectance and aerosol retrievals in biomass burning region of Brazil. *Geosci. Remote Sens. Lett.,* **3**, 169-172.

Wen, G., A. Marshak, and R. F. Cahalan, L. A. Remer, and R. G. Kleidman, 2007: 3D aerosol-cloud radiative interaction observed in collocated MODIS and ASTER images of cumulus cloud fields. *J. Geophys. Res.,* **23**, xxxx, doi: 10.1029/2006JD008267.

Zhang, J., J. S. Reid, B. N. Holben, 2005: An analysis of potential cloud artifacts in MODIS over ocean aerosol optical thickness product. *Geophys. Res. Lett.,* **32**, 10.1029/2005GL023254.

Zhuravleva, T., and A. Marshak, 2005: On the validation of the Poisson model of broken clouds. *Izvestiya Atmos. and Oceanic Phys.*, **41**, 6, 713-725.

Figures

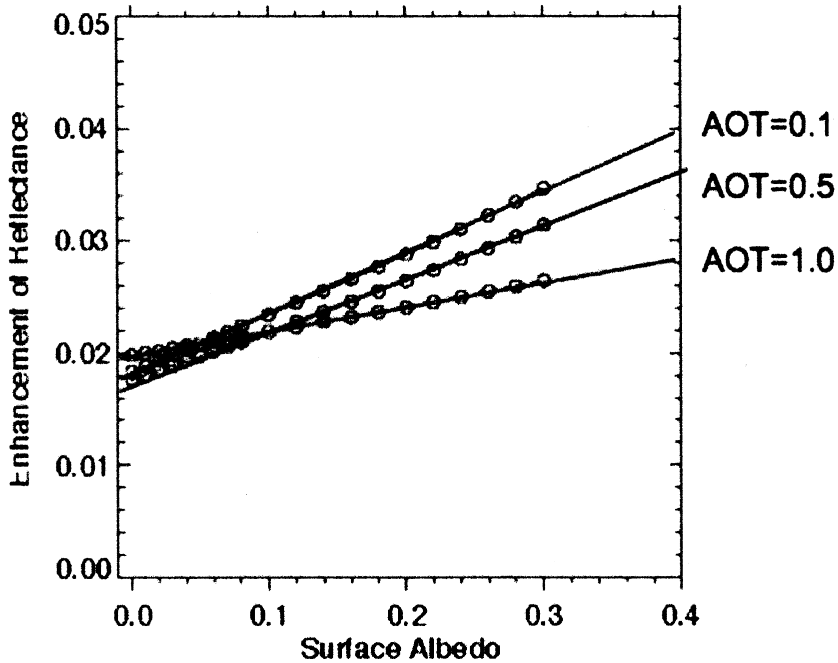

Figure 1. Cloud-induced enhancement as a function of surface albedo and AOT for a broken cumulus scene with cloud cover close to 50% described in Wen et al. (2007). The Rayleigh scattering is for 0.47 μm.

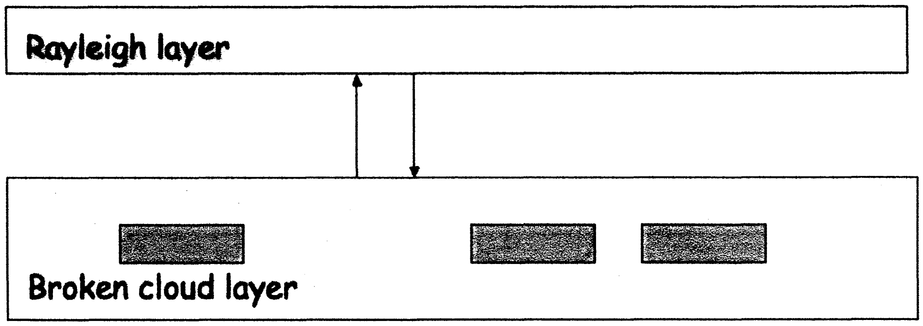

Figure 2. A schematic two-layer model of a broken cloud field (lower layer) and Rayleigh scatterers (upper layer).

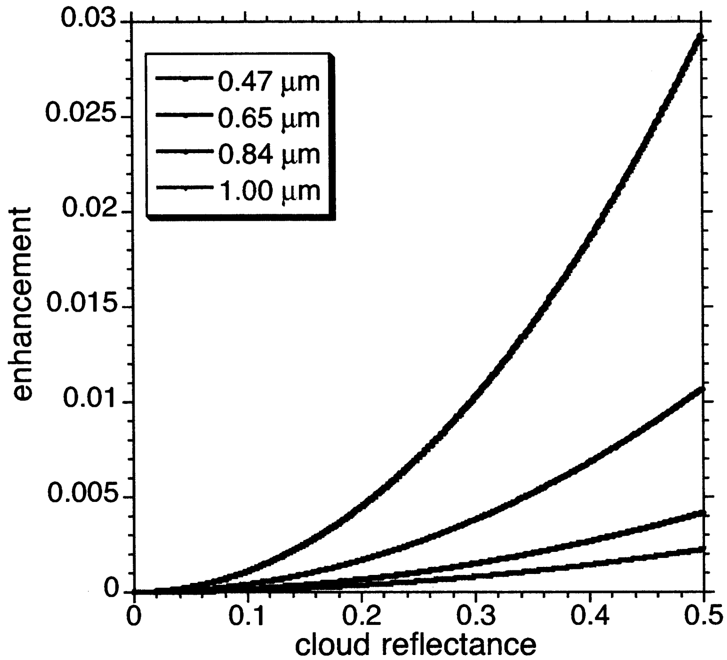

Figure 3. Cloud-induced enhancement as a function of cloud reflectance for four wavelengths: 0.47, 0.65, 0.84, and 1.00 µm. The Rayleigh optical depth is taken to be 0.05 at 0.65 µm and varies inversely with the fourth power of the wavelength. The solar zenith angle, $\theta_0 = 60^{\circ}$, viewing zenith angle $\theta = 0^{\circ}$, and the surface is black.

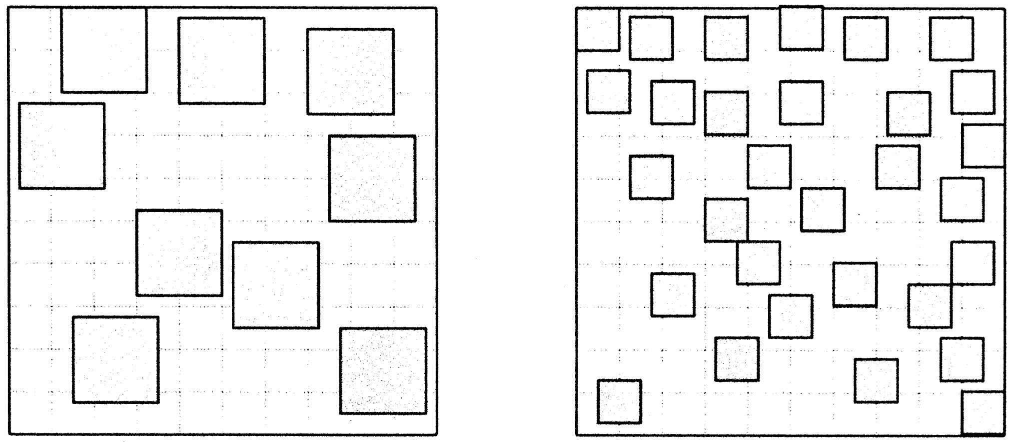

Figure 4. An example of the Poisson distribution of broken cloud fields with cloud fraction $A_c = 0.3$ for a 10 by 10 km area. For a cloud vertical thickness of 1 km, the left panel has cloud aspect ratio $\gamma = 0.5$, and the right panel has $\gamma = 1$.

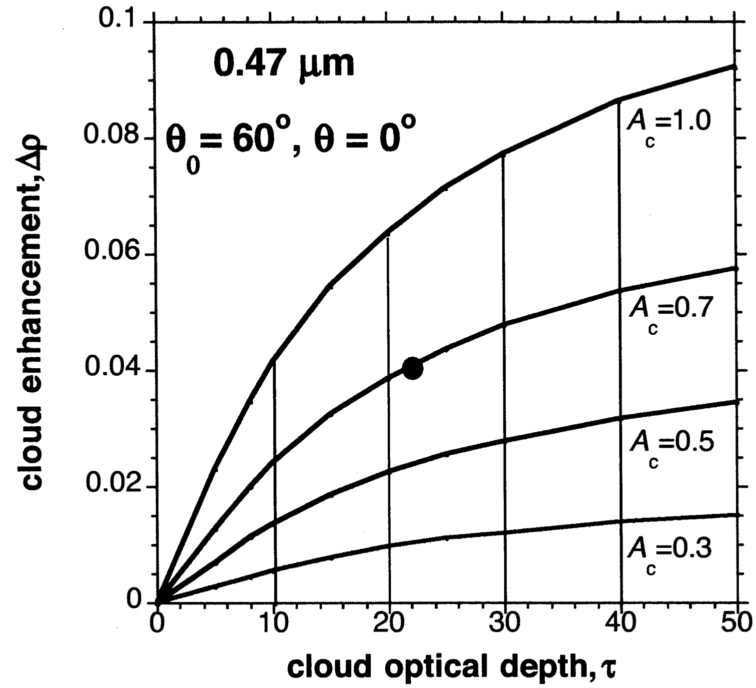

Figure 5. Cloud-induced enhancement $\Delta\rho$ and cloud optical depth τ for four cloud fractions, A_c = 1.0, 0.7, 0.5, and 0.3. $A_c = 1$ corresponds to the plane-parallel approximation. The aspect ratio is $\gamma = 1$, solar zenith angle, $\theta_0 = 60°$, view zenith angle, $\theta = 0°$, and the surface is black. The filled circle indicates the expected cloud-free radiance enhancement due to nearby clouds with $\tau = 22$ and $A_c = 0.7$.

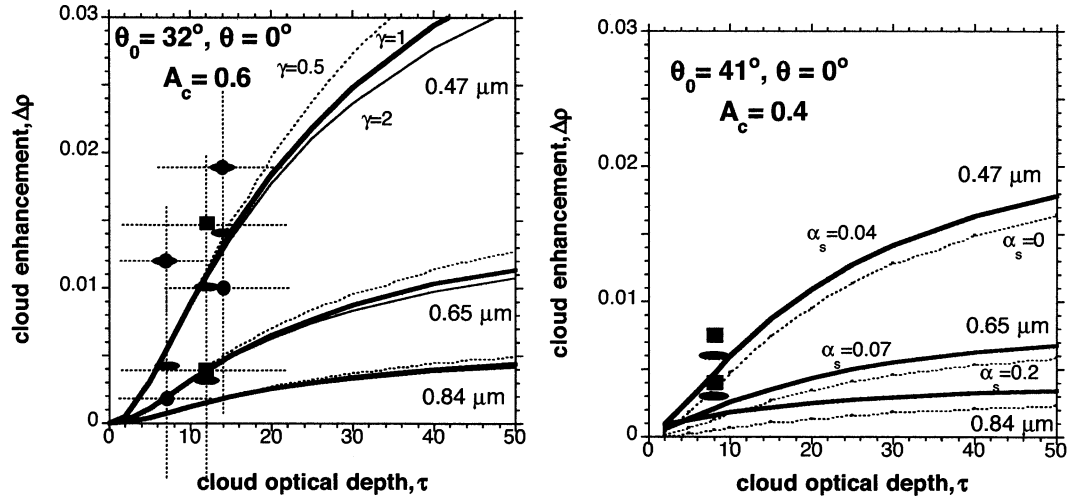

Figure 6. Cloud-induced enhancement $\Delta\rho$ and cloud optical depth, τ, for three wavelengths: 0.47, 0.65, and 0.84 μm. **(Left)** Cloud fraction, $A_c = 0.6$, solar zenith angle, $\theta_0 = 32°$, and view zenith angle, $\theta = 0°$. These conditions correspond to the first broken Cu scene studied by Wen et al. (2007). Thick solid lines are $\Delta\rho$ calculated using (2)-(4) with aspect ratio $\gamma = 1$, dotted lines are with $\gamma = 2$, and thin solid lines with $\gamma = 0.5$. The surface is black. Filled blue and red squares, circles and ovals are from Wen et al. (2007) at 0.47 and 0.66 μm. Squares correspond to the scene average values; circles correspond to two subscenes with thick and thin clouds, and ovals correspond to asymptotic values. The dotted lines coursing through the symbols give one standard deviation. **(Right)** Cloud fraction, $A_c = 0.4$, solar zenith angle, $\theta_0 = 41°$, and view zenith angle, $\theta = 0°$. These conditions correspond to the second broken Cu scene studied by Wen et al. (2007) and by Marshak et al. (2006). The aspect ratio $\gamma = 1$. Dotted lines are $\Delta\rho$ calculated using (2)-(4) for a black surface. Solid lines are for the $\Delta\rho$ that correspond to the MODIS-retrieved surface spectral albedos: $\alpha_s = 0.04$ at 0.47 μm, $\alpha_s = 0.07$ at 0.65 μm, and $\alpha_s = 0.2$ at 0.84 μm. Filled ovals and squares are also from Wen et al. (2007). Ovals correspond to the actual asymptotic values while squares are the average enhancements for those pixels that were selected by the MODIS AOT retrieval algorithm (see text for details).

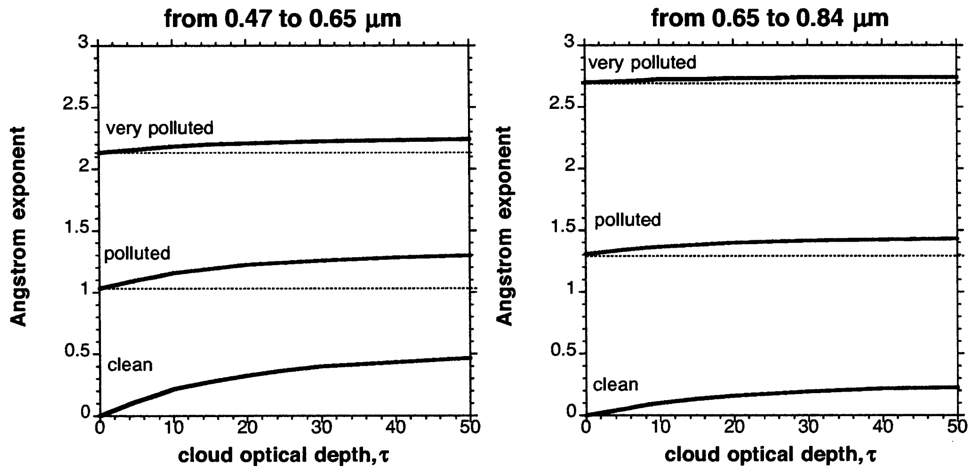

Figure 7. The Angström exponent and cloud optical depth, τ, for three situations: "clean," "polluted," and "very polluted." The cloud fraction is $A_c = 0.5$, the aspect ratio, $\gamma = 0.5$, and the illumination and viewing directions are the same as in Fig. 5. Two spectral intervals are shown: **left** panel is for 0.47 and 0.65 μm while **right** panel is for 0.65 and 0.84 μm.